

Fabio Falchi^{1,2,*} and Salvador Bará¹

¹ *Dept. de Física Aplicada, Universidade de Santiago de Compostela, 15782 Santiago de Compostela, Galicia*

² *Istituto di Scienza e Tecnologia dell'Inquinamento Luminoso (Light Pollution Science and Technology Institute), 36016 Thiene, Italy.*

Keywords: Light pollution, Environmental assessment, Astronomical observatories, Spatial planning, Lighting

*Author for correspondence (falchi@istil.it).

ABSTRACT

Light pollution modelling and monitoring has traditionally used zenith sky brightness as its main indicator. Several other indicators (e.g. average sky radiance, horizontal irradiance, average sky radiance at given interval of zenith distances) may be more useful, both for general and for specific purposes of ecology studies, night sky and environmental monitoring. These indicators can be calculated after the whole sky radiance is known with sufficient angular detail. This means, for each site, to integrate the contribution in each direction of the sky of each light source in the radius of hundreds of km. This approach is extremely high time consuming if the mapping is desired for a large territory. Here we present a way to obtain maps of large territories for a large subset of useful indicators, bypassing the need to calculate first the radiance map of the whole sky in each site to obtain from it the desired indicator in that site. For each indicator, a point spread function (PSF) is calculated from the whole sky radiance maps generated by a single source at sufficiently dense number of distances from the observing site. If the PSF is transversally shift-invariant, i.e. if it depends only on the relative position of source and observer, then we can further speed up the map calculation via the use of fast Fourier-transform (FFT). We present here examples of maps for different indicators. Precise results can be calculated for any single site, taking into account the site and light sources altitudes, by means of specific inhomogeneous (spatially-variant) and anisotropic (non rotationally symmetric) PSFs.

1. Introduction

Light pollution is raising in magnitude and extension in the World (Kyba et al., 2017) and also in the scientific literature production. Its negative consequences are evident in numerous fields, including astronomy, environment, tourism, cultural heritage, energy usage.

Its control and abatement is consequently a rising issue. The traditional way used to limit its consequences has been to work on the single sources, imposing parameters to be followed to keep their polluting impact low. However low the impact of a single light source is, the cumulative load of all contributing light polluting sources on the night environment is not regulated. For this reason, it is fundamental to implement the complementary approach of introducing cap limits on the pollutant factor (Falchi et al. 2011; Falchi 2018). Artificial light impact on the night sky and environment has been recently formalized (Bará & Lima 2018; Falchi & Bará 2020), introducing in the light pollution abatement policies the de-facto standard in environmental protection for air quality policy and management since the second half of last century (Hayes 2018).

To help controlling the light pollution levels several indicators have been proposed. The most widely used is the zenith brightness (e.g.: Cinzano et al. 2001; Falchi et al. 2016a), but others may be of greater interest to assess the quality of the night sky and night environment: average radiance in the whole night sky, average radiance at 30° above the horizon, average radiance in the first 10° above the horizon, total horizontal irradiance, average vertical irradiance, maximum radiance at a particular zenith distance or in the whole sky hemisphere, and others (some are discussed in Duriscoe 2016).

2. Light pollution indicators

The spectral radiance [$\text{W sr}^{-1} \text{m}^2 \text{nm}^{-1}$] gives all the information we need to obtain the values of the indicators used to determine the light pollution impact on the environment, human and animal physiology, animal behaviour, astronomy, landscape and so on. The radiance integrated over the action spectrum of interest (e.g. scotopic, photopic and melanopic curves in humans, different astronomical photometric bands, action spectra of various taxa, see Longcore et al. 2018) gives us the radiance in a specific band. In our examples here we used the Johnson-Cousin V band, the historically most used band in light pollution modelling, with an effective wavelength $\lambda=550 \text{ nm}$.

The artificial radiance indicators we choose are: zenith radiance, average hemispheric radiance, average radiance at 60° zenith distance, average radiance with zenith distance greater than 80° , horizontal irradiance. The zenith radiance is the most commonly used in light pollution literature. It is the easiest also to obtain with portable ‘point and shot’ instruments (e.g. SQM-L), even if, strictly speaking, what is obtained by these instruments is an average weighted by the sensitivity off centre in the field of view of the instrument. The artificial zenith brightness becomes harder and harder to measure as we approach pristine sky conditions. As we necessarily collect, beside the artificial sky brightness, also the natural component that in dark-sky locations is preponderant. To obtain the artificial component, it is necessary to subtract a good estimation of the natural background given by natural airglow, Milky Way, stars, and zodiacal light including Gegenshein (Duriscoe 2013, Masana 2021). This indicator, moreover, tends to underestimate the pollution in a site, as near zenith, on average, we find the less light polluted part of the night sky.

The average hemispheric radiance gives a better description of the overall night sky conditions, weighting equally the radiance seen in every direction in the upper hemisphere. This indicator is equivalent, apart from eventual scaling constant factor to the various definitions of ‘scalar irradiance’ (or scalar illuminance, in case we use the photopic sensitivity curve to weight the spectral irradiance).

The average artificial radiance at 60° zenith distance (i.e. at 30° above the horizon) gives the average contamination at what it is commonly assumed the lowest normal pointing direction of telescopes in professional astronomy research. The Recommendations of the International Astronomical Union, adopted in the late seventies of last century, allowed for a 10% maximum increase of radiance at 45° zenith distance in every azimuth, over the lowest natural light conditions, in any part of the spectrum from 300 nm to 1000 nm (Smith F.G., in Cayrel 1979). As our indicator is averaged over all azimuths, we suggest to compute it at the lower normally used pointing direction (60° zenith distance, instead of 45°). To have the real situation at each azimuth, a computation of the sky radiance in every direction should be performed. Anyway, the average radiance at 60° zenith distance is a good indicator for the scientific usability of the sky at astronomical observatory sites.

The average radiance at zenith distance greater than 80° (i.e. in the first 10° above the horizontal) is a useful indicator for evaluating the impact of light pollution on the night landscape, both for humans (e.g. fruition of Natural Parks during the night) and animals (e.g. phototaxis), as for terrestrial animals the average pointing direction of the eyes is along the horizon, so the most influential part of the radiance coming from the sky is that in the first degrees above the horizon. This may not be true for other fauna (e.g. zooplankton), for which the following indicator seems more adequate.

The horizontal irradiance gives the surface density of the energy flux arriving on a horizontal surface from the whole sky. This is an indicator used in ecology studies, as it is useful both for flora and fauna. Moreover, if we assume that the surface receiving the light is Lambertian (a fairly good approximation in most cases) and has a reflectance ρ , then its radiance is obtained multiplying the irradiance by ρ and dividing by π . This gives an idea of the perceived brightness of the environment. The mean of the average hemispheric radiance (in the upper hemisphere) and the radiance (in the lower hemisphere), computed from the irradiance on the ground, gives the 4π averaged radiance perceived by animals moving in the environment.

3. Computation of light pollution indicators

3.1. The Garstang-Cinzano light propagation model

To perform the computations of the indicators, we used the model of light propagation in the atmosphere developed by Garstang (Garstang 1986 and 1989) and Cinzano (Cinzano et al. 2000, 2001, Cinzano & Elvidge 2004). This model takes into account for: (i) altitude of the observing site, (ii) altitude of the source, (iii) transparency of the atmosphere, (iv) shape of the intensity of the source, (v) extinction and double scattering correction, (vi) screening due to Earth curvature. The band used for the computation is the Johnson-Cousin V, but the model can be adapted for different bands (e.g. Johnson-Cousin B, or the R, G and B used in common digital cameras, animal vision including human photopic and scotopic bands). See the Appendix A for details on the assumed atmospheric model and on the upward emission function of the light sources.

3.2. Hemispheric sky map radiance from a single source

We computed the hemispheric maps of the radiance produced by a single light emitting source in the sky of an observer located at distances from 0.12 km to 527 km. The hemispheric maps present the radiance in 100593 points in the sky, chosen to be uniformly distributed in a square lattice in a Zenith Equal Area (ZEA) projection, so that each elemental area in the map corresponds to the same solid angle in the sky (Calabretta 2002). In our case each area measures about 0.2 square degree, the same of the full Moon or the Sun. This density is more than sufficient to detect even the steepest gradients in sky brightness (Bará & Falchi, in prep.), which usually are found near the horizon (e.g. in the direction of a bright source, such as an isolated city). Figure 1 shows the hemispheric radiance maps for clarity parameter $K'=1$, for the Upward Emission Function (UEF) used in the New World Atlas of Artificial Night Sky Brightness, hereafter NWA (Falchi et al 2016a) in the first row and for the Lambertian, middle angles and low angles UEFs for three different distances produced by a point-like source.

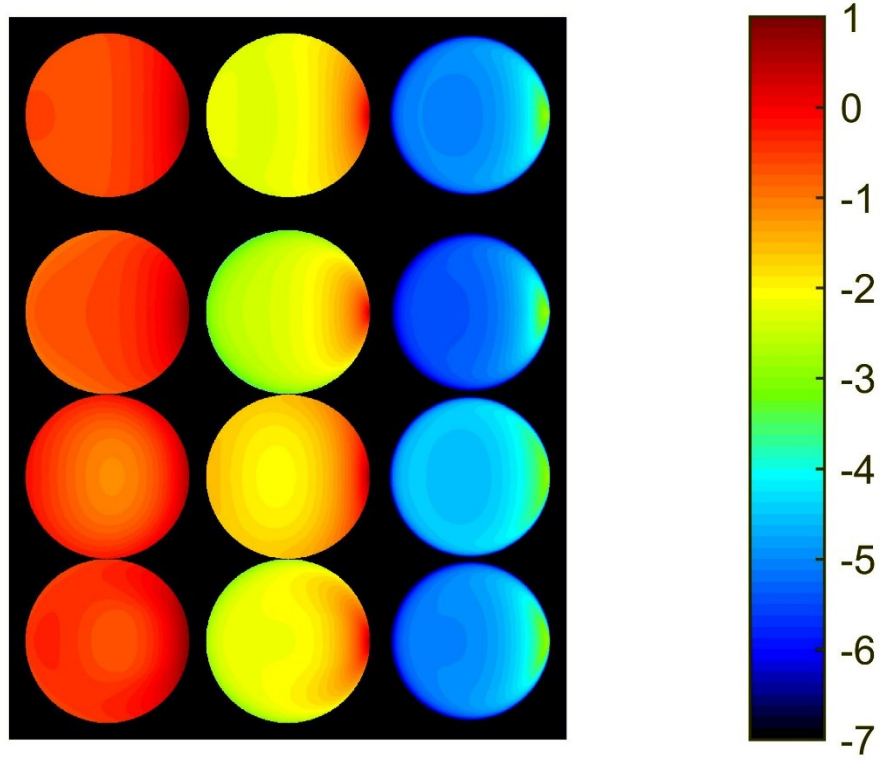


Figure 1. Radiance of the sky hemisphere obtained for 1 km (1st column), 10 km (2nd column) and 100 km (3rd column) distances from a point source with the Upward Emission Function used for the NWA (1st row), for a Lambertian UEF (2nd row), for low angles UEF (3rd row) and for middle angles UEF (4th row). The scale is in arbitrary logarithmic radiance units.

3.3. Calculating the indicators and their PSF

A great advantage of the ZEA projection is that it makes easy to compute indicators from the data points. For example, the average radiance of the whole night hemisphere is the simple sum off all the computed values divided by the number of values, in our case, 100593. To have the average radiance in the first ten degrees above the horizon, we just need to select and count the number of points with zenith distance greater than 80 degrees. For the average radiance at 30°, we made the average of the radiances for points between 29° and 31° above the horizon.

To get the horizontal irradiance E we compute:

$$E = \frac{2\pi}{N} \sum_i \cos \theta_i B_i(2)$$

where B_i is the artificial radiance of the i -th point, θ_i is its zenith distance, and $2\pi/N$ is the solid angle element (sr) in the upper hemisphere, being N the total number of points computed in the sky using a uniform ZEA lattice.

The PSFs are very smooth functions of the distance from the source, so it is not necessary to compute their value at high distance density. In our case we computed the PSFs values with distance steps increasing by a factor of 1.2, so that the range distance 0.12 km to 527 km was covered by 47 steps.

For PSFs with fixed site and sources altitudes, the numerical PSFs were best fitted by a polynomial of degree 6 in a log PSF vs log distance representation. When PSFs for different altitudes of sources were needed, the numerical PSFs obtained for several different sources altitudes were used to find a degree 4 polynomial best fit of the above mentioned coefficients of the degree 6 polynomial. The analytical expressions of the fitted PSFs have, in this last case, 35 coefficients (Bará and Falchi, in prep.).

For each indicator we computed its PSF for three different upward source emission functions and then linearly combined them using the same coefficients found in the NWA. The PSFs are shown in Figure 2.

The computation of the PSF of an indicator, compared to the computation of the radiance in all the necessary directions in the sky and then, from the obtained all-sky radiance maps, compute the desired indicator, gives a relevant computation time-saving of the order of the number of points in the sky necessary to compute the indicator itself. For the case of the average hemispheric radiance with the angular resolution used by us, this time-saving is in the order of 10^5 . For fewer points or lower resolution, the time-savings are proportionally smaller, and the estimation errors increase.

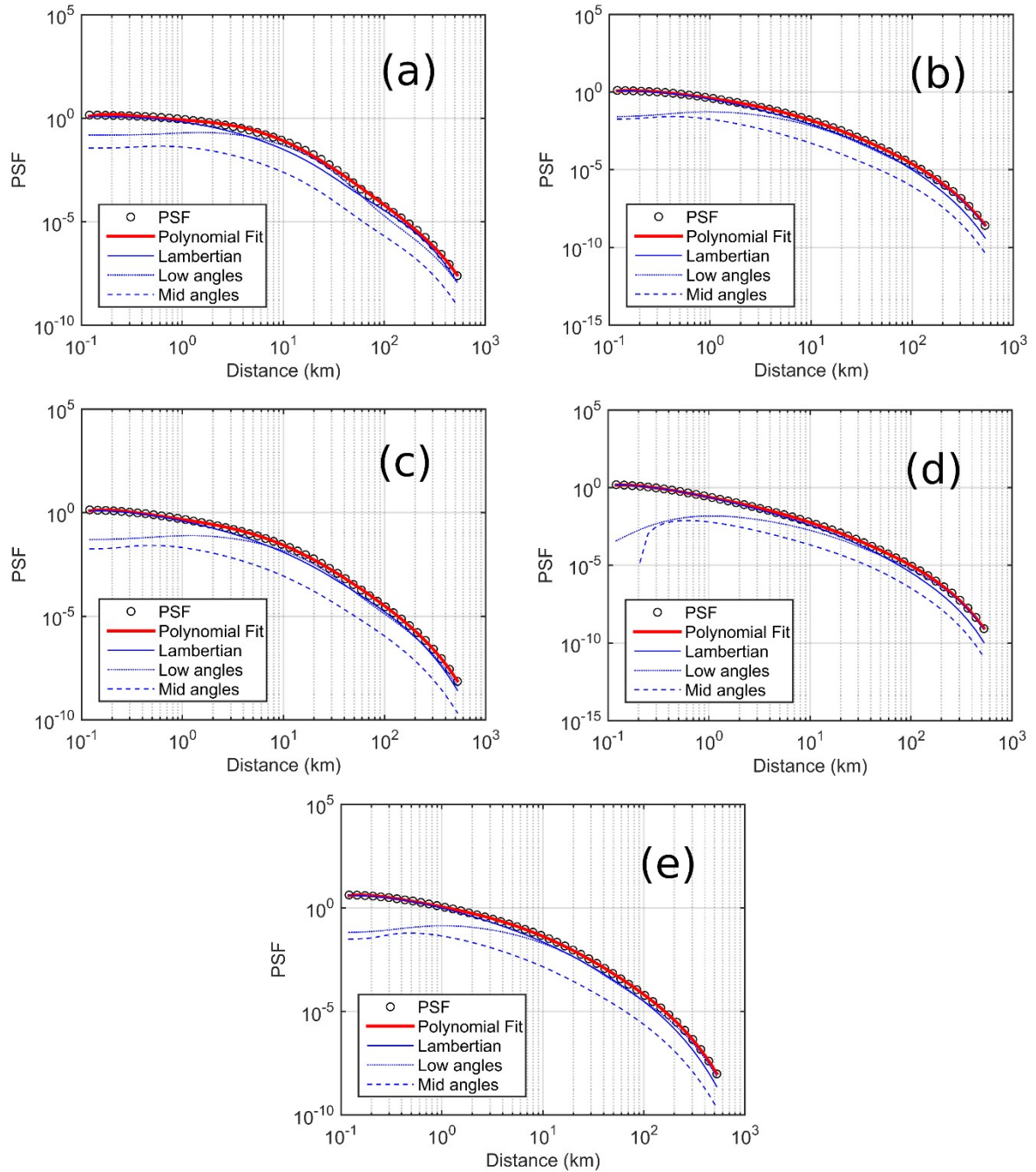


Figure 2. Radial dependence of the rotationally symmetric point spread functions of several light pollution indicators, for the sources and observing site altitudes described in section 4, as a function of the distance to the sources. (a) Average radiance below

10° above horizon; (b) Average radiance between 29°-31° degrees above horizon; (c) Average all-sky radiance (upper hemisphere); (d) Zenith radiance; (e) Horizontal irradiance. PSF in arbitrary linear units, $K=1$. The circles correspond to the total PSF, evaluated from the all-sky radiance data. The thick red line displays the analytical fit (log polynomial). The thin blue lines correspond to the three angular source emission modes included in our particular realization of the general model: Lambertian (full line), low-angles (dotted line), and mid-angles (dashed line).

4. Maps of indicators for large territories

Following the method introduced by Bará et al. 2020 we computed, to exemplify the use of indicators, the maps of Iberian Peninsula for the artificial zenith sky radiance, the average hemispheric radiance, the average radiance in the first 10 degrees above the horizon, and the horizontal irradiance, all in the Johnson-Cousin V band. We assumed:

- A vertically layered, shift-invariant atmosphere (see section 3.1.1) with clarity parameter $K'=1$ (evaluated at sea level);
- A 626 m constant altitude for the sites (average altitude of Iberian Peninsula);
- A 282 m constant altitude for the light sources (average of the altitude of the sources weighted by their VIIRS-DNB radiances);
- An azimuthally symmetrical upward emission function with zenith dependence determined by the same parameters used in the NWA (section 3.1.2).

Under these conditions, often implicitly assumed in most of light pollution propagation studies, we can compute a single PSF for all sites and can apply the FFT – iFFT path to compute the maps, having a huge time saving in computation times due to the combined savings due to the computation of PSF of indicators (section 3.4) and the use of FFT. For the dimensions of the map of light sources (about 4000 pixels wide) and of the PSF (about 2000 pixels wide), the gain in computation time is of the order of 10^4 (see Bará et al, 2020 for details). The combined overall time gain is therefore of the order of 10^9 . Note that this gain in computation time allows for relaxing one or more of the conditions above, to eventually affine the simulations (e.g. producing PSF for different altitudes and applying them in the relevant territories).

As input map for light sources we used the is the 2015 Annual VNL V1 "vcm-orm-ntl" (VIIRS Cloud Mask - Outlier Removed - Nighttime Lights) annual composite, excluding any data impacted by stray light, with ephemeral lights and background (non-lights) set to zero (Elvidge et al., 2017). The GeoTIFF file is in EPSG:4326, geographic Latitude/Longitude projection with 15" wide pixels. We reprojected it to EPSG:25830, ETRS 89/ UTM 30N to have equal area pixels of 409 m side over the region of interest.

The maps produced were calibrated by comparing the map of the zenith sky brightness with the map of the NWA (Falchi et al, 2016b). See Appendix B for details.

For the maps of Iberian Peninsula we used, as reference for the natural radiance values, the GAia Map of the Brightness Of Natural Sky (GAMBONS, Masana et al, 2021, <https://gambons.fqa.ub.edu>), updated to Gaia EDR3. The data used as input in the GAMBONS model are shown in Table 2. For a pristine reference natural sky, we averaged the indicators' 24 values obtained approximately every 15 days for a whole year, obtained for a site at 40 N on the meridian 0 at the local midnight (U.T.= 0). The results are the same for all location at 40 N at local midnight. The graphs of Figure 3 show the variation of the reference values during the year. It is interesting to note that the radiance around zenith has the greatest variations along the year, following the proximity of the Milky Way to zenith itself, with the brightest zenith peak values about two times higher than the lowest. Nonetheless, the yearly mean of the zenith radiance is very close to the mean of the all sky radiance. This is substantially different to the artificial radiance behaviour, where at zenith is usually at its minimum.

Location coordinates	Altitude (m)	Natural Airglow	Aerosols Ångstrom exponent (α)	Aerosol optical thickness τ
Lon.: 0 W Lat.: 40.0 N	626	100%	1.0	0.21

Table 1. Parameters used to evaluate the reference night sky radiance with The GAia Map of the Brightness Of Natural Sky (GAMBONS).

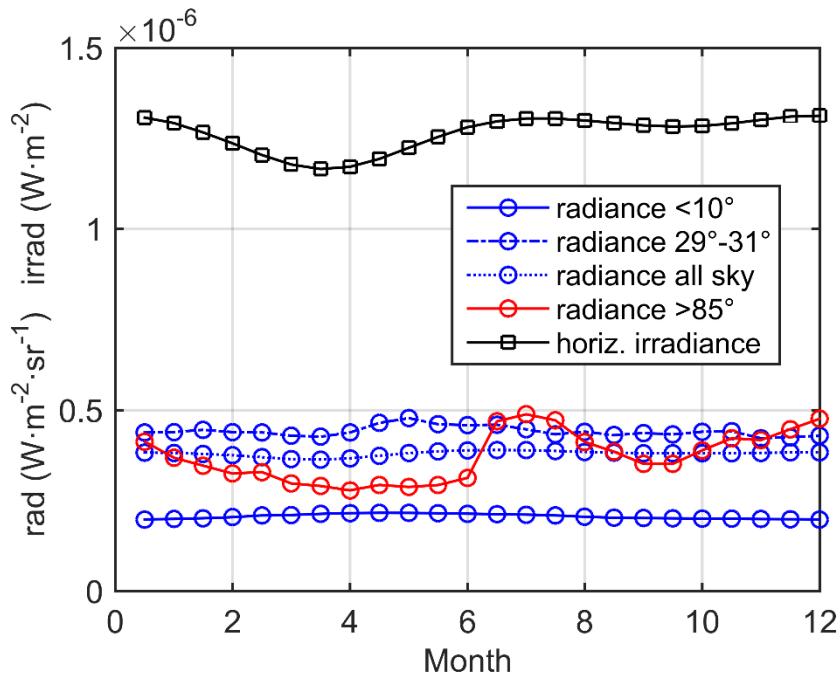


Figure 3. The night sky reference values values in function of the date of the year for a location at 40°N and the parameters shown in Table 2.

The reference values of the indicators, computed from GAMBONS with the parameters of Table 2 are summarized in Table 3. Please note that the reference values are necessarily different for the various indicators. Curiously, the average zenith sky radiance and the average all sky radiance differ in this case by only 2%. The natural sky near the horizon is darker than elsewhere. This is usually the opposite behaviour of what happens with the artificial radiance, usually lower at zenith and higher along the horizon.

Indicator (Johnson-Cousin V band):	Zenith radiance ($\text{W m}^{-2} \text{sr}^{-1}$)	Average 30° radiance ($\text{W m}^{-2} \text{sr}^{-1}$)	Average all sky radiance ($\text{W m}^{-2} \text{sr}^{-1}$)	Average radiance below 10° ($\text{W m}^{-2} \text{sr}^{-1}$)	Horizontal irradiance (W m^{-2})
Reference value:	3.718×10^{-7}	4.418×10^{-7}	3.802×10^{-7}	2.066×10^{-7}	$1,2643 \times 10^{-6}$

Table 2. Reference radiances and irradiances chosen for expressing the light pollution indicators as dimensionless relative values.

The colour codes used in the maps are relative to the reference values of Table 3. Each colour step indicates a doubling in the artificial radiance, starting from black (<1% of the reference value), to dark grey (1%-2%), light grey (2%-4%), and so on up to the white level (>41 times greater than the reference).

The different radiance indicators maps in Figure 4 show that even the portions of the Iberian Peninsula that are still relatively dark at zenith, present in reality a much heavier overall impact by light pollution than might have been expected. In particular, the average radiance in the sky hemisphere shows that the darkest sky in the entire peninsula is 15% brighter than the reference natural sky, while the same ratio using the zenith radiance gives a less alarming 4% increase. The average radiance in the first 10 degrees above the horizon, probably the best indicator to show the impact on the landscape perception, gives an even worse situation, as the darkest place has an average artificial radiance 65% higher than the reference natural radiance along the horizon. This situation is evident in the lower right map of Figure 4, in fact the light green level indicates artificial radiance from 64% to 128% of the reference, so the darkest areas in the peninsula have the horizon about two times brighter than the chosen reference conditions. As this indicator gives the mean radiance along all the 360° horizon, the peak values will be necessarily higher in the direction(s) pointing toward the main source(s) of pollution. While the colour code is the same used in the NWA, a comparison, even in the case of the zenith map, must take into account the substantial difference in the reference natural value used in this work (yearly averaged zenith radiance with average natural skyglow) and in the NWA (22.00 V magnitude, corresponding to a zenith pointing in the direction of the north galactic pole and with relatively low natural airglow).

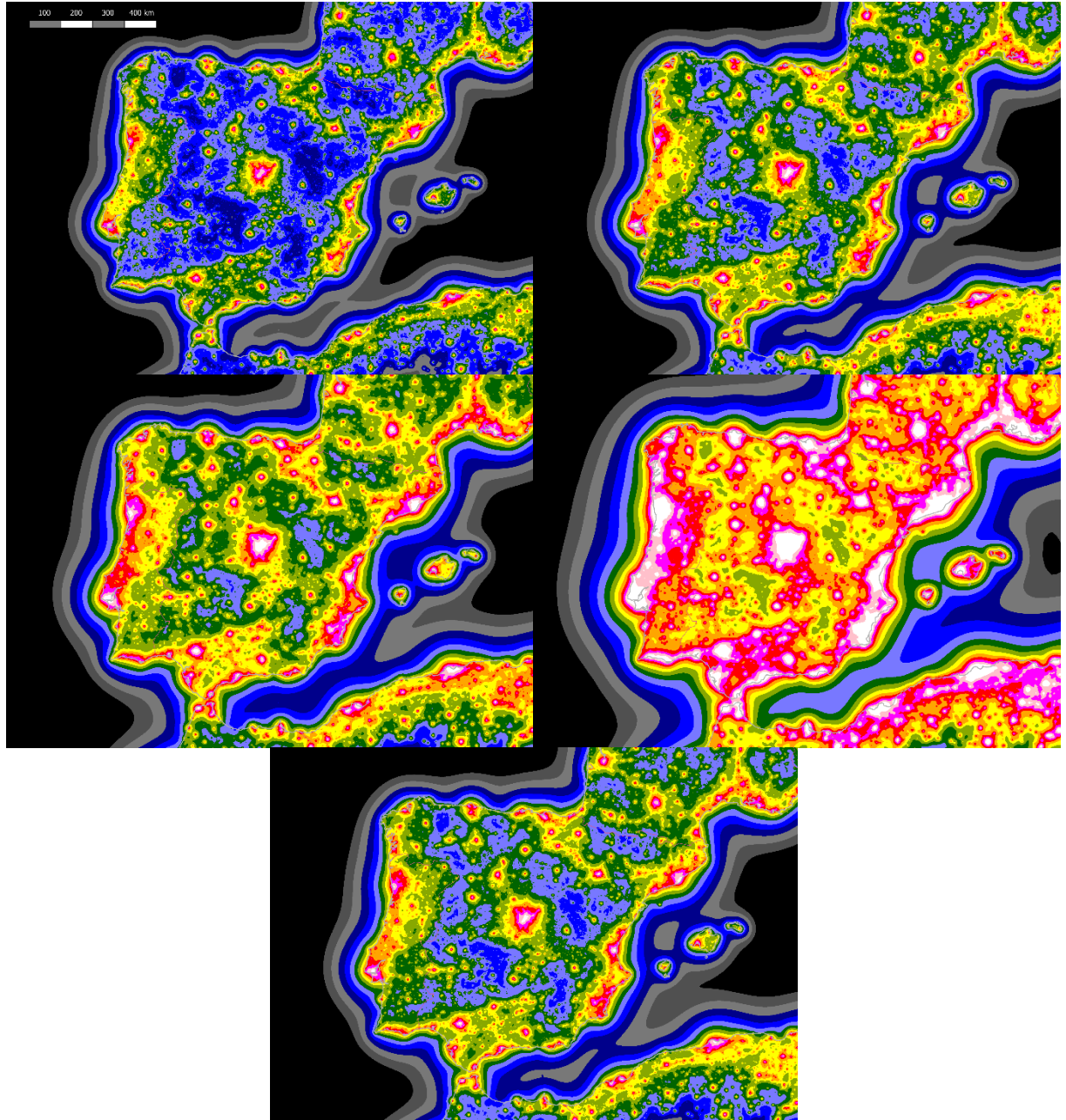


Figure 4. Maps of the zenith artificial radiance (upper left), average radiance at 29° – 31° above the horizon (upper right), average hemispheric radiance (central left) and average radiance in the first 10° above the horizon (central right). The bottom line map shows the horizontal irradiance (note that its aspect is very close to that of the average radiance at 29° – 31°). Colours indicate the ratio, for each indicator, between the artificial radiance or irradiance and the reference values assumed for average pristine conditions.

5. Indicators for a single site

To compute with more accuracy the values of the indicators for a single site, and to determine the relative contribution of each elementary patch of the territory to their final value, we used the 35 parameters analytical best fit polynomial described section 3.3. To take advantage of the PSFs that take into account for sources' altitude, we used the Global Multi-resolution Terrain Elevation Data (GMTED2010) by the USGS and the National Geospatial-Intelligence Agency (Danielson and Gesch 2011). In figure 5 we show the spatial weighting function for the average all sky radiance in a 3D colour coded representation. To obtain the indicators value in an observing site, we multiply this weighting function, describing the contribution of a unit valued light source in each pixel, by the VIIRS data value of the corresponding pixel; i.e. we perform a pixel wise multiplication of the two rasters. This will give us a raster with the contribution of each pixel source to the indicator in the selected observing site. Summing all the values of each pixel gives finally the value of the indicator.

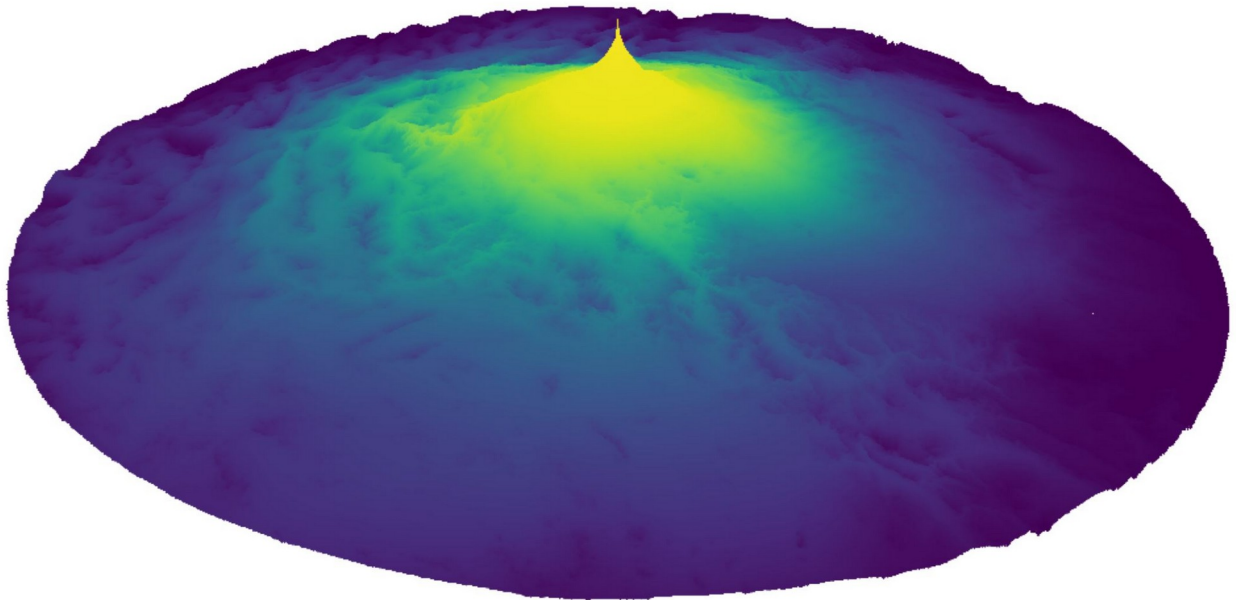


Figure 5. Weighting function describing the contribution to the all sky averaged sky brightness in Powell Memorial (Grand Canyon National Park, USA) of a unit-radiance source located in its surroundings for a radius of 400 km. The effect of the altitude of the light sources, superimposed to that of the distance from centre, is clearly visible in this false colour 3D rendering.

The graphs in figure 6 show the cumulative light sources contributions in a radius of 500 km to three indicators, the zenith radiance, the average all sky radiance and the average radiance in the first 10° above the horizon at Moran Point (left and central graphs) and at Powell Memorial Point (right graph). The first thing, apparent from the left graph is, as expected, that the zenith radiance is far lower than both the average all sky radiance and, more so, the average radiance just above the horizon. The second thing, better visible in the central graph, is that the relative contribution of the light sources depends on the indicators. In fact, for the zenith sky radiance, the main contributors are at about 20 km from the Moran Point overlook, and corresponds to Grand Canyon Visitor Center, Village, airport and Tusayan. These sources contribute to more than 40% to the zenith sky radiance at Moran Point. Another 40% contribution comes from sources located from about 48 km to 250 km. There is also a not negligible contribution of nearly 20% due to sources in the 250 to 310 km, due to the cities of Phoenix and Las Vegas. These two cities are the main contributors to both the average all sky radiance (40% of the total) and, of course, to the pollution of the first degrees above the horizon, as half the radiance in this part of the sky is due to these two sources. This shows that the wilderness experience of being in a national park may be compromised by pollution coming more than 250 km away. The right graph shows what happens in a relatively close site, Powell Memorial, about 20 km from Moran Point, but much closer to Grand Canyon Village. Here the main contributors to the sky radiance are the close sources, in the very first kilometres. Nonetheless, a not negligible relative contribution is given also by Phoenix and Las Vegas, especially toward the horizon, even if they span in azimuth only about 20° toward the South and 10° toward WNW respectively. Note that we computed the average radiance in the first 10° above the horizon over all the 360° of azimuth.

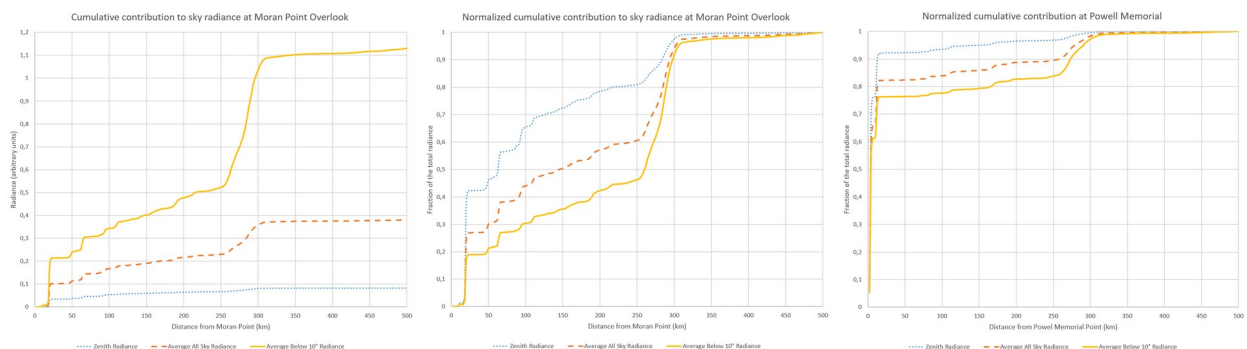


Figure 6. The cumulative indicators radiance in function of the distance of the site to the light sources for Moran Point, left and center, and Powell Memorial point, right. In the left graph is easily visible that the zenith sky radiance is about 1/5th of the average all sky radiance and 1/14th of the average radiance in the first 10° above the horizon. In the central and right graphs, each indicator is normalized to 1 at 500 km to show the relative contribution to each indicator of the sources at various distances.

6. Conclusion

We proposed a method to calculate several indicators of interest in light pollution studies and policy control, bypassing the need to previously calculate the artificial radiance in a great number of directions in the whole sky hemisphere. These indicators give a better tailored evaluation of the night sky and environment for particular protection needs (e.g. for professional astronomy, for wilderness ‘sensation’ in natural parks and protected areas during the night, for ecological impacts on wildlife). Consequently, the ‘red lines’ policy of controlling the light pollution (Falchi & Bará 2020) has a wide array of indicators to be used, even cumulatively. For example, an area can be protected by imposing values not to be surpassed for different indicators. For each indicator, the bigger polluters can be identified, both at pixel level (of about 0.2 km² in case of VIIRS detected radiance) or at the appropriate administrative level (e.g. municipality, county, province) in order to take actions for reentering in the parameters. The proposed method can become the standard for controlling and limit light pollution on the night sky and on night environment.

Acknowledgments

We thank to the Gaia team at Universitat de Barcelona for providing us access to the full stand-alone GAMBONS run-time code for the computation of the reference indicators (Masana et al, 2021).

Funding Statement

SB acknowledges support from Xunta de Galicia grant ED431B 2020/29.

Data Accessibility

All data sources used in this work are in the public domain. No additional materials would be required to conduct an attempt at replication. VIIRS-DNB composites are available, among other options, from <https://payneinstitute.mines.edu/eog/> and <https://earthobservatory.nasa.gov/images/event/79869/earth-at-night>.

The GMTED2010 Digital Elevation Maps are available here: https://topotools.cr.usgs.gov/gmted_viewer/viewer.htm

Competing Interests

We have no competing interests.

Authors' Contributions

Both Authors contributed equally to this work.

Appendix A

A.1 Atmospheric model

The atmosphere is assumed to be in hydrostatic equilibrium with the number density N_m of the air molecules decreasing exponentially with the altitude h :

$$N_m(h) = N_{m,0} e^{-ch}$$

where $N_{m,0} = 2.55 \times 10^{19} \text{ cm}^{-3}$ is the molecular density at sea level and $c = 0.104 \text{ km}^{-1}$ is the inverse scale height (Garstang 1986). Also the aerosol vertical distribution decreases exponentially with altitude:

$$N_a(h) = N_{a,0} e^{-ah}$$

where $N_{a,0}$ is the aerosol density at sea level and a is its inverse scale height. To allow for different atmospheric transparency conditions we use the clarity parameter K' defined at sea level (see Cinzano and Elvidge 2004):

$$K' = \frac{N_{a,0} \sigma_a}{N_{m,0} \sigma_m 11.11}$$

where σ_a is the aerosol scattering cross-section and σ_m is the molecular scattering cross-section. To obtain the clarity parameter at other altitudes, for a given ground level H , we get the K as originally defined by Garstang:

$$K = K' e^{(c-a)H}$$

The relation between a and K is $a=0.657 + 0.059K$. We performed the computations for $K'=1$. Values of three different K' (0.5, 1 and 2) and the corresponding other atmospheric parameters (see Garstang 1986) are shown in table A1.

The aerosol scattering phase function follows that of Garstang (Garstang 1991, equations 5) and can easily be modified with other phase functions.

Clarity parameter K'	Inverse scale height a (km^{-1})	Optical thickness τ	Horizontal visibility (km)	Astronomical extinction at zenith in V band (magnitudes)
1	0.716	0.306	26.1	0.332

Table A3. Some parameters for describing the atmosphere compared to the clarity parameter used in this work.

A.2 Upward emission function

We performed the computations using a three parameters upward emission function (UEF), following Cinzano & Falchi 2012:

$$I_{up}(\varphi) = \frac{a_1 \cdot 2 \cos \varphi + a_2 \cdot 0.5543 \varphi^4 + a_3 \cdot q 1.778 \cos(3\varphi - \frac{\pi}{3})}{2\pi} (1)$$

where I_{up} is the intensity of the source (W/sr), assumed azimuthally symmetric, φ is the zenith angle measured in the source reference frame, and a_1 , a_2 , and a_3 are three coefficients that allows to obtain a wide variety of upward emission functions. The function can be normalized by dividing each of these parameters by the sum of all three coefficients. For zenith distances smaller than 30° we impose $q=0$ so that the term with the a_3 parameter is null. With both a_2 and a_3 equal to zero, I_{up} becomes Lambertian. With $a_1=0.574$ and $a_2=0.426$ we get the ‘standard’ Garstang upward function (with his parameters $G=0.15$ of ground albedo and $F=0.1$ of fraction of direct upward flux from the luminaires). With $a_1=0.757$, $a_2=0.212$ and $a_3=0.031$ we have the upward function used in the new World Atlas of Artificial Night Sky Brightness, with the parameters found with the best fit with the sky brightness measurements (Falchi et al. 2016a).

Appendix B

Johnson V values of the night sky brightness are often expressed in astronomic $\text{mag}_V/\text{arcsec}^2$. This system of reporting requires defining the precise shape of the V band (Bessell 1990) as well as choosing a 'zero-point' for decrypting the magnitudes and converting them into physical quantities with a clear meaning. The use of the magnitude system creates many unnecessary difficulties, since very often researchers do not clearly state the zero point used to report their results: AB, Vega 0.00, Vega +0.03, if Vega then with which spectrum, etc.

The measured physical quantity is always the radiance (either in energy or in photon numbers) recorded within the Johnson V band. The native choice for Johnson V is to use radiance in energy units. So, a patch of the sky has m_V $\text{mag}_V/\text{arcsec}^2$ if its radiance L_V within the Johnson V band is:

$$L_V = L_{0V} \times 10^{-0.4 \times m_V} (b1)$$

The value of the constant L_{0V} depends on the scale chosen for the m_V system.

If m_V is measured in the Vega scale, assigning to Vega a V magnitude of +0.03 and using Vega's STIS003 spectrum, then (Masana et al, 2021)

$$L_{0V} = 143.1685 \text{ W m}^{-2} \text{ sr}^{-1} (b2)$$

Other spectrum choices would give rise to slightly different L_{0V} values, as e.g. $140.6 \text{ W m}^{-2} \text{ sr}^{-1}$ if using Allen's choice for the Sun spectrum (Allen 1973; Bará 2017) or $146.8 \text{ W m}^{-2} \text{ sr}^{-1}$ if using Rieke's spectrum for Vega (Rieke et al, 2008; Bará et al, 2020).

For our work, consistent with the Gaia-Hipparcos map scale (Masana et al, 2021), the linear physical quantity associated with m_V mag_V/arcsec² in the Vega 0.03 system will then be the radiance:

$$L_V = 143.1685 \times 10^{-0.4 \times m_V} W m^{-2} sr^{-1} (b3)$$

Calibrating Garstang-Cinzano V band zenith brightness PSFs

The Garstang-Cinzano PSFs in arbitrary linear units were calibrated for the New World Atlas, NWA (Falchi et al, 2016) using large datasets of SQM measurements. The maps we produce now using the same fortran code as used for the NWA can be calibrated by matching the corresponding zenith brightnesses calculated both ways. There is a slight difference in the definition of the PSFs we are using. Ours is for variable source altitude and fixed observer altitude in the case of the computation for a single site. In the case of the maps of the Iberian Peninsula we used a fixed average altitude for the observers (i.e. all the observers are put at the same altitude above sea level, the average altitude of the peninsula) and a fixed altitude for the sources (obtained by weighting their altitudes by their VIIRS-DNB radiances), while the NWA had sea-level sources and variable observer altitudes.

The rationale for absolute radiant calibration of the Garstang-Cinzano PSF is:

- Assume that commercial SQM magnitudes per square arcsecond are equivalent to Johnson V magnitudes per square arcsecond in a Vega +0.03 system.
- Convert the V magnitudes into in-band radiances using Eq. (b3) above.
- Determine the best fitting constant linking the zenith brightness maps calculated with the Garstang-Cinzano arbitrary units PSF and the NWA results, averaging over the appropriate territory.

References

- Bará S, Lima RC, Photons without borders: quantifying light pollution transfer between territories, *International Journal of Sustainable Lighting* 20(2), 51-61 (2018) DOI :10.26607/ijsl.v20i2.87
- Bará S, Falchi F, Furgoni R, Lima RC. **Fast Fourier-transform calculation of artificial night sky brightness maps**, *Journal of Quantitative Spectroscopy & Radiative Transfer* 240 (2020a) 106658, doi: <https://doi.org/10.1016/j.jqsrt.2019.106658>
- Bará S. Black-body luminance and magnitudes per square arcsecond in the Johnson-Cousins BVR photometric bands. *Photonics Letters of Poland*, 11(3), 63-65 (2019). <https://dx.doi.org/10.4302/plp.v11i3.926>
- Bará S., Aubé M., Barentine J., Zamorano, J. Magnitude to luminance conversions and visual brightness of the night sky. *Monthly Notices of the Royal Astronomical Society*, 493, 2429–2437 (2020b). <https://doi.org/10.1093/mnras/staa323> Green open access: <http://arxiv.org/abs/2002.01494>
- Bessell, M.S. (1990). UBVRi passbands. *Publications of the Astronomical Society of the Pacific*, 102, 1181-1199.
- Calabretta M.R., Greisen E.W., 2002, **Representation of celestial coordinates in FITS**, *Astronomy and Astrophysics* 395, 1077-1122. doi: 10.1051/0004-6361:20021327
- Cinzano, P. Falchi, F., Elvidge, C.D., Baugh, K.E, ‘The artificial night sky brightness mapped from DMSP satellite Operational Linescan System measurements’, *Mon. Not. R. Astron. Soc.*, Volume 318, Issue 3, 1 November 2000, p.641. <https://doi.org/10.1046/j.1365-8711.2000.03562.x>
- Cinzano P., Falchi F., Elvidge C. D. (2001). **Naked-eye star visibility and limiting magnitude mapped from DMSP-OLS satellite data**, *Mon. Not. R. Astron. Soc.* 323, 34–46
- Cinzano P, Falchi F, Elvidge C. 2001 The first world atlas of the artificial night sky brightness. *Mon. Not. R. Astron. Soc.*, **328**, 689–707.
- Cinzano P., Elvidge C. D. (2004). **Night sky brightness at sites from DMSP-OLS satellite measurements**, *Mon. Not. R. Astron. Soc.* 353, 1107–1116 doi:10.1111/j.1365-2966.2004.08132.x
- Cinzano P., Falchi F. (2012). **The propagation of light pollution in the atmosphere**, *Mon. Not. R. Astron. Soc.* 427, 3337–3357. doi:10.1111/j.1365-2966.2012.21884.x
- Danielson, J.J., and Gesch, D.B., 2011, Global multi-resolution terrain elevation data 2010 (GMTED2010): U.S. Geological Survey Open-File Report 2011–1073, 26 p
- Duriscoe DM. **Measuring Anthropogenic Sky Glow Using a Natural Sky Brightness Model**. *Publications of the Astronomical Society of the Pacific*, 2013; 125(933):1370-1382. DOI:10.1086/673888

- Duriscoe, D.M. (2016). Photometric indicators of visual night sky quality derived from all-sky brightness maps. *Journal of Quantitative Spectroscopy & Radiative Transfer*, 181, 33–45. DOI:10.1016/j.jqsrt.2016.02.022
- C. D. Elvidge, K. Baugh, M. Zhizhin, F. C. Hsu, and T. Ghosh, “VIIRS night-time lights,” *International Journal of Remote Sensing*, vol. 38, pp. 5860–5879, 2017.
- Falchi F., Cinzano P., Elvidge C.D., Keith D.M., Haim A., 2011, Limiting the impact of light pollution on human health, environment and stellar visibility, *Journal of Environmental Management* 92, 2714–2722
- Falchi F, Light Pollution in Urban Pollution: Science and Management, Susanne M. Charlesworth and Colin A. Booth (Editors), ISBN: 978-1-119-26050-9, Oct 2018, Wiley-Blackwell DOI:10.1002/9781119260493.ch11
- Falchi F, Bará S. 2020. A linear systems approach to protect the night sky: implications for current and future regulations. *R.Soc. Open Sci.* 7: 201501. <https://doi.org/10.1098/rsos.201501> accepted version available in <https://arxiv.org/abs/2008.09928>
- Falchi F, Cinzano P, Duriscoe D, Kyba CCM, Elvidge CD, Baugh K, Portnov BA, Rybnikova NA, Furgoni R. 2016a The new world atlas of artificial night sky brightness. *Sci. Adv.* 2, e1600377. (doi: 10.1126/sciadv.1600377)
- Falchi, Fabio; Cinzano, Pierantonio; Duriscoe, Dan; Kyba, Christopher C. M.; Elvidge, Christopher D.; Baugh, Kimberly; Portnov, Boris; Rybnikova, Nataliya A.; Furgoni, Riccardo (2016b): Supplement to: The New World Atlas of Artificial Night Sky Brightness. V. 1.1. GFZ Data Services. <https://doi.org/10.5880/>
- Garstang RH. 1989. Night-sky brightness at observatories and sites. *Publ Astron Soc Pac* **101**, 306-329.
- Garstang, R. H. (1986). **Model for artificial night-sky illumination**. Publications of the Astronomical Society of the Pacific, 98, 364-375.
- Garstang, R. H. (1991). **Dust and light pollution**. Publications of the Astronomical Society of the Pacific, 103, 1109-1116
GFZ.1.4.2016.001
- Hayes E, Evolution of Air Quality Policy and Management in Urban Areas in Urban Pollution: Science and Management, Susanne M. Charlesworth and Colin A. Booth (Editors), ISBN: 978-1-119-26050-9, Oct 2018, Wiley-Blackwell DOI:10.1002/9781119260493.ch03
- Longcore T, Rodríguez A, Witherington B, Penniman JF, Herf L, Herf M. 2018. Rapid assessment of lamp spectrum to quantify ecological effects of light at night. *J Exp Zool.* vol. 329, pp. 511–521. <https://doi.org/10.1002/jez.2184>
- Masana E, Carrasco JM, Bará S, Ribas SJ. A multi-band map of the natural night sky brightness including Gaia and Hipparcos integrated starlight. *Monthly Notices of the Royal Astronomical Society* (in press, 2021)
- Oke, J.B., Gunn, J.E. (1983). Secondary standard stars for absolute spectrophotometry. *The Astrophysical Journal*, 266, 713-717
- Smith F.G. in Cayrel, R. (1979). 50. Identification and Protection of Existing and Potential Observatory Sites. *Transactions of the International Astronomical Union*, 17(1), 215-223. doi:10.1017/S0251107X00010798

